8

Wave Optics of Synchrotron Radiation

Nikolay Smolyakov
National Research Center "Kurchatov Institute", Moscow, Russia

1. Introduction

Synchrotron radiation is a unique source of infrared radiation being highly polarized, pulsed, with the broad emission band and about thousand times brighter than standard thermal source. All just mentioned synchrotron radiation adventures apply to a large choice of experimental techniques and investigations. Among them are high-pressure studies, earth science and biology, microspectroscopy, reflectance and absorption spectroscopy for surface study, time-resolved spectroscopy and ellipsometry. Interest in infrared synchrotron radiation goes back to the 1980s (Duncan & Williams, 1983). At present numerous infrared beamlines have been developed at synchrotron radiation facilities throughout the world, see, e. g., (Bocci et al., 2008; Carr & Dumas, 1999; Guidi et al., 2005; H. Kimura et al., 2001; S. Kimura et al., 2001; S. Kimura et al., 2006; Roy et al., 2006; Williams & Dumas, 1997). Efforts to improve the radiation beam characteristics lead to elaboration more and more sophisticated beamline optics. To achieve this goal, we need to know all characteristics of emitted radiation, its intensity distribution, polarization and phase distribution. In particular, the synchrotron radiation wave properties play a major role in conventional diagnostics of electron beams in storage rings (Andersson et al., 2006; Elleaume et al., 1995; Fang et al., 1996; Flanagan et al., 1999; Hs & Huang, 1993; Weitkamp et al., 2001). In this case, the image of the electron beam is formed by an optical lens. The synchrotron radiation diffraction on the lens iris aperture restricts the resolution of the beam profile measurements. Infrared synchrotron radiation was used for longitudinal beam diagnostics at FLASH free electron laser (Grimm et al., 2008; Paech et al., 2006, 2007). Recent trends show an increased usage of synchrotron radiation interferometers for high precision measurements of the electron beam sizes (Artemiev et al., 1996; Chubar, 1995; Hiramatsu et al., 1999; Katoh & Mitsuhashi, 1999; Naito & Mitsuhashi, 2010). For proper interpretation of observed data, we also need to know synchrotron radiation phase distributions.

As far as we know, the paper (Sabersky, 1973) was one of the first papers to pioneer the investigation of geometrical-optical properties of synchrotron radiation coming from the curving relativistic electron beam. The phase-space techniques, commonly applied to charged beam optics, was used for analysis. The focusing of synchrotron radiation by a convex lens within the framework of geometrical optics was considered in (Green, 1976; Ogata, 1987). The qualitative agreement with the experimentally observed data was found, although the quantitative discussion needs taking into account of the diffraction effects. The synchrotron radiation treatment as a laser-like Gaussian beam with a small opening angle was performed in (Coisson & Marchesini, 1997; Kim, 1986; Ogata, 1991; Takayama et al.,

1998, 1999). The important benefit to the use of this approximation is that the Gaussian beams have been much studied. It has been shown however that the Gaussian approximation has some limitations when calculating the synchrotron radiation coherence. At the same time the Gaussian beam approximation can reasonably be applied to the horizontally polarized component of synchrotron radiation only. It has been also found that the Gaussian beam approximation is poor for undulator radiation (Kim, 1986). In addition, as it was noted (Miyahara & Kagoshima, 1995), the brightness function defined by Kim can be negative (that has no physical meaning) and should therefore be modified.

The most-used scheme of diffraction phenomena implementation into synchrotron radiation theory was suggested by A. Hofmann and F. Meot (Hofmann & Meot, 1982). This technique involves the following steps. First, the synchrotron radiation from a single electron has supposedly the phase distribution of a point source that is spherically symmetrical one, while its amplitude distributions (for both horizontal and vertical polarizations) should be identical to that of an electron in a homogeneous magnetic field. Under these assumptions and supposing small observation angles, for such source we can calculate the Fraunhofer diffraction pattern. Then, assuming that we have a transverse Gaussian distribution of such point-like sources, and that they are not coherent (it corresponds to incoherent radiation of different electrons in the beam), we can calculate the image distribution by a convolution of the single-electron radiation diffraction pattern with the point sources distribution. Assume further that, instead of moving relativistic beam, we have a uniform longitudinal distribution of such immobile point sources along the circular trajectory of the beam, which are again incoherent. Then we can calculate the resultant image distribution from the electron beam by straightforward integration along longitudinal coordinate. This scheme is relatively simple, easy-to-interpret physically and allows easily estimating the optical resolution for the beam cross-section measurements. It was employed by a number of groups for optimization of the electron beam profile monitor systems and experimental date interpretations, e.g. (Andersson & Tagger, 1995; Arp, 2001; Clarke, 1994; Hs & Huang, 1993). The main weakness of this method is that some steps in this scheme are not deduced from the fundamental principles of radiation theory that is to say from the Maxwell equations. Close inspection of this model shows that some assumptions seem not sufficiently self-consistent. Thus, considering the synchrotron radiation as the radiation from the immobile point sources distributed uniformly along electron's trajectory, we in fact presume that the radiation, generated by the electron at neighboring sections of its path, are incoherent, but this is not the case. The simplest counter example is undulator radiation, where the radiation, emitted by the electron at different periods (5-10 and more cm in length), is coherent. Accordingly, there is no reason to expect the opposite for synchrotron radiation. Rather, we should expect that the radiation from different parts of the electron trajectory is coherent in the case of synchrotron radiation as well.

In terms of wave optics a consistent definition of the problem is as follows. Let a physical device consists of multiple optical parts. Each part has characteristics known beforehand. It is sufficient to know the radiation wave amplitude and phase at every point of the device entrance window in order to take advantage of the Helmholtz - Kirchhoff integral theorem (Born & Wolf, 1986). If these values are known, one can calculate the distribution of the radiation intensity on the device output screen.

The analysis of synchrotron radiation phase distribution based on the fundamental radiation principles was presented at the Eleventh Russian Conference on the usage of Synchrotron Radiation (Novosibirsk, 1996) (Smolyakov, 1998a, 1998b). Using exact solutions of the Maxwell

equations, the expansion of the synchrotron radiation phase in powers of small observation angles was obtained. A leading quadratic term of this expansion shows that synchrotron radiation by its phase distribution nature is much closer to the radiation emitted by an immobile point source rather than to the longitudinally extended source according to the geometrical-optical approach mentioned above. At the same time the correction cubic term produces a self-aberration effect of synchrotron radiation. The synchrotron radiation exhibits a searchlight effect which manifests itself in the amplitude distribution non-homogeneity in the vertical direction. Using the known amplitude and phase distributions, the intensity distribution of the focused synchrotron radiation from one electron (single electron image) was computed (Smolyakov, 1998c). The effect of the lens aperture on the optical resolution of the electron beam profile measurement system by means of synchrotron radiation was also analyzed. Later the similar results were obtained in the paper (Bosch, 1999), in the part which deals with the synchrotron radiation focusing by a reflecting sphere with an aperture.

An accurate simulation of synchrotron radiation propagation through the beamline optical system inevitably needs the application of specialized computer codes. Nowadays two codes are mostly in use: the code SRW (Chubar & Elleaume, 1998) and the code PHASE (Bahrdt, 1997, 2007). Comparison studies of these codes may be found in (Bowler et al., 2008). Some distributions of focused synchrotron radiation with and without phase corrections were simulated with the help of SRW (Chubar et al., 1999, 2001).

The codes, which are based on the wave propagation, are precise but time consuming. It should be mentioned that simpler and hence faster approaches are also used for analysis of beamline optical system properties (Ferrero et al., 2008).

In this chapter we will consider solely the case of standard synchrotron radiation, namely, the radiation generated by highly relativistic electrons while they pass through the uniform magnetic field of bending magnets in storage rings. Intensity distributions of synchrotron radiation, as well as its polarization properties, have been studied quite intensively and are widely covered in the literature. The amplitudes of horizontally (σ) and vertically (π) polarized wave components of synchrotron radiation are expressed in terms of modified Bessel functions. Although the first formulas for the wave amplitudes were derived more than 60 years ago, regular study of the synchrotron radiation phase distributions started relatively recently, about dozen years ago and not yet analyzed in full measure. Here an exact expression for the phase distribution in synchrotron radiation wave will be derived. Surprisingly, the resultant exact formula is written in terms of elementary functions only, though this formula is rather cumbersome. The lens aperture effect on the focused radiation intensity distribution is analyzed.

We do not consider edge radiation in this chapter. A comprehensive list of papers on edge radiation can be found in (Geloni et al. 2009a, 2009b; Korchuganov & Smolyakov, 2009; Smolyakov & Hiraya, 2005).

2. Qualitative analysis of synchrotron radiation wave properties

2.1 Wave optics of convex lens

To gain greater insight into physics of synchrotron radiation wave optics, let us consider a standard case of the point source radiation focusing by a refractive lens, see Fig. 1. Within

the framework of geometrical optics, the set of rays (R_1 and R_2) from the point source P, located at a distance $D > 0$ ahead of the lens, is focused to an image point S aft of the lens at the distance L so that: $1/D + 1/L = 1/f$, where f is the focal length of the lens.

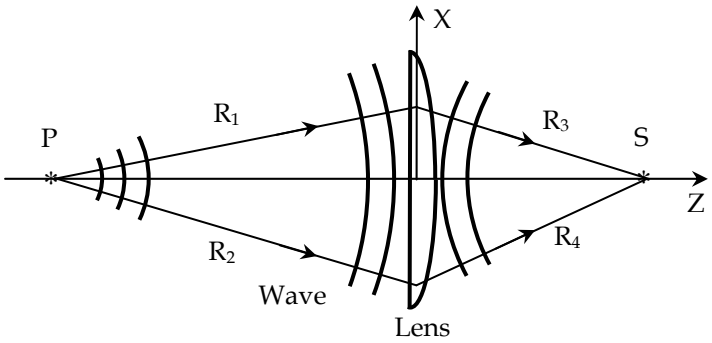

Fig. 1. Point source radiation focusing by a lens: P - point source, S - its image, R_1 - R_4 - radiation rays.

In terms of wave optics, a point source emits a divergent spherical wave $\vec{E}(x,y,z) = \frac{\vec{E}_0}{r} e^{ikr}$, with the spherically symmetric amplitude and phase distributions. Here $k = 2\pi/\lambda$, $r = \sqrt{x^2 + y^2 + (z+D)^2}$. In its passing through the ideal lens, the wave does not change its amplitude distribution (no absorption) while the phase distribution is transformed from the divergent-type one into the convergent-type wave as it is shown in Fig. 1. This is due to the fact that the lens, with its spherical shape and correspondently with smoothly varied thickness, imparts the proper different phase delays to different parts of the incident wave. Supposing that the lens sizes are far less than the distance to the source D, we have for the incident wave at $z = 0$:

$$\vec{E}_{in}(x,y,z=0) = \frac{\vec{E}_0}{D} \exp\left(ikD + ik(x^2 + y^2)/(2D)\right). \tag{1}$$

After passing the ideal infinitely thin lens with the focal length f, the correspondent distributions of the outgoing wave $\vec{E}_{out}(x,y,z=0)$ at $z = 0$ will be equal to:

$$\vec{E}_{out}(x,y,z=0) = \vec{E}_{in}(x,y,z=0) \cdot \exp\left(-ik(x^2 + y^2)/(2f)\right). \tag{2}$$

Here the phase factor $\exp\left(-ik(x^2 + y^2)/(2f)\right)$ describes the action of the lens on the radiation passing through it. With a knowledge of the radiation distributions $\vec{E}_{out}(x,y,z=0)$ aft of the lens and applying the Kirchhoff integral theorem (Born & Wolf, 1986), we can calculate the radiation intensity at any point of the observation screen $\{x_s, y_s, z_s\}$ at $z_s > 0$.

$$\vec{E}(x_s, y_s, z_s) = \frac{-i}{\lambda} \int_A \vec{E}_{out}(x, y, z=0) \frac{\exp(ikr_s)}{r_s} dxdy\,, \tag{3}$$

where $r_s = \sqrt{(x-x_s)^2 + (y-y_s)^2 + z_s^2} \cong z_s + \frac{(x-x_s)^2 + (y-y_s)^2}{2z_s}$ is the distance of the lens element $dxdy$ from the point $\{x_s, y_s, z_s\}$ at the observation screen and the integral is taken over the lens aperture A. The standard simplification of the Kirchhoff integral was made by neglecting the small terms of the order of λ/D, λ/L and λ/f. The expression (3) displays the well-known Huygens-Fresnel Principle: every point of a wave front $\vec{E}_{out}(x, y, z=0)$ may be considered as a center of a secondary disturbance which gives rise to spherical waves $\frac{\exp(ikr_s)}{r_s}$. The total disturbance at the observation point $\{x_s, y_s, z_s\}$ is the result of all these secondary waves interference.

Substituting Eq. (1) and Eq. (2) into Eq. (3), we get:

$$\vec{E}(x_s, y_s, z_s) = \frac{-i\vec{E}_0}{\lambda D z_s} \int_A \exp\left((ik/2)\left(\frac{1}{D} + \frac{1}{z_s} - \frac{1}{f}\right)\left(x^2 + y^2\right)\right) \cdot \exp\left(\left(-ik/z_s\right)\left(xx_s + yy_s\right)\right) dxdy \tag{4}$$

Assume for simplicity that the lens is rectangular in shape: $|x| \le l_x$, $|y| \le l_y$, where $2l_x$ and $2l_y$ are the lens horizontal and vertical sizes respectively. Considering the integral (4) in the image plane $z_s = L$, where $1/D + 1/L - 1/f = 0$, we get:

$$\vec{E}(x_s, y_s, z_s = L) = \frac{-4i\vec{E}_0}{\lambda DL} l_x l_y \frac{\sin(\xi_s)}{\xi_s} \cdot \frac{\sin(\eta_s)}{\eta_s}\,, \tag{5}$$

where $\xi_s = \frac{2\pi l_x}{\lambda L} x_s$, $\eta_s = \frac{2\pi l_y}{\lambda L} y_s$. The radiation intensity is proportional to $\left|\vec{E}(x_s, y_s, z_s)\right|^2$. Notice that the focused spot has horizontal and vertical sizes $\lambda L / l_{x,y}$ respectively, which are in inverse proportion to the lens aperture sizes $2l_{x,y}$. Second, the radiation intensity at the spot center $x_s = 0$, $y_s = 0$, is proportional to $l_x^2 l_y^2$. It is physically clear that with the lens horizontal aperture $2l_x$ increasing, the photon flux through the lens varies proportionally and the horizontal size of the spot is correspondently diminished. So, the density is quadratic in $2l_x$. Similar to the vertical aperture $2l_y$.

2.2 Time-domain analysis of synchrotron radiation

Here, we will consider synchrotron radiation in the time domain and describe it in terms of electric field of the emitted wave and its arrival time to an observer. A relativistic electron generates synchrotron radiation in the uniform magnetic field of a storage ring bending magnet. Let us consider a physical experiment with a geometry shown in Fig. 2. The electron rotates anticlockwise.

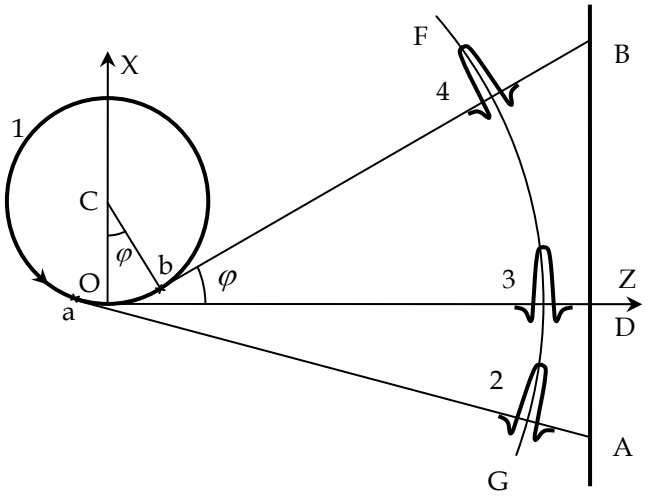

Fig. 2. Typical layout of synchrotron radiation observation: 1 – electron trajectory; 2, 3, 4 – synchrotron radiation field pulses; A-D-B – device entrance window.

For simplicity, we will restrict here our qualitative analysis to the case of radiation in the storage ring median plane XOZ. Briefly, the idea of analysis is as following.

In uniform magnetic field, an electron generates synchrotron radiation homogeneously along its orbit. In the median plane on which the electron moves, the wave shape of the emitted radiation (the electric field temporal structure, curves 2, 3 and 4 in Fig.2) is the same at any observer positions in this plane (e.g., points A, D and B) provided the distances from the emitting points a, O and b respectively to the observers are the same. In the strict sense the distances aA, OD and bB are slightly different from each other. Here, however, this difference can be neglected being negligibly small in comparison with the distance itself. The difference in the field between observers A, D and B is in the relative arrival time τ_A, τ_D and τ_B of the radiation field. The distinctions $\Delta\tau$ between arrival time τ_A, τ_D and τ_B cannot be neglected since the quantity $c\cdot\Delta\tau$ is not negligibly small as compared with the radiation wavelength, where c is the speed of light. This arrival time difference gives rise to the phase difference in the frequency domain.

Let a relativistic electron moves along its circular orbit in a horizontal plane XOZ (the magnetic field is aligned with the vertical Y-axis). It is convenient to choose a frame of reference in such a way that at the initial moment $t=0$ the electron was at the origin of the coordinates with its velocity vector directed along the Z- axis. Then the equations of the electron motion are:

$$\begin{aligned} r_x(t) &= R - R\cos(\Omega t), \\ r_y(t) &= 0, \\ r_z(t) &= R\sin(\Omega t). \end{aligned} \tag{6}$$

$$\begin{aligned}\beta_x(t) &= \beta\sin(\Omega t),\\ \beta_y(t) &= 0,\\ \beta_z(t) &= \beta\cos(\Omega t).\end{aligned} \tag{7}$$

Here, R is the electron orbit radius, Ω is the angular velocity of the electron $\Omega = c\beta/R$, β is the electron reduced velocity $\vec{\beta}(t) = \frac{1}{c}\cdot\frac{d\vec{r}(t)}{dt}$, $\beta = \left|\vec{\beta}(t)\right| = const$, c is the speed of light.

Let us consider a points at the observation screen (plane A-D-B, device entrance window), which is transversal to the *Z*-axis. The observer, who is at the point $\{0,0,D\}$, will detect the peak in the electric field distribution of the radiation wave (synchrotron radiation field pulse) at the moment $\tau = D/c$. This is obvious because, at time $t = 0$ the electron was at the origin of coordinates, and the vector of its velocity pointed to the observer with coordinates $\{0,0,D\}$. If there are other observers located at some different points *A* or *B* of the observation screen, they will detect a similar synchrotron radiation pulse. Nevertheless, these observers will detect the signal peak at different instants. Obviously, the time detected by each observer consists of two components. The first part $t_e(x_s)$ is the time, when the electron was at such point of its orbit $\vec{r}(t_e)$ from where the velocity vector pointed to the observer with coordinates $\vec{X}_s = \{x_s,0,D\}$ (points *a* or *b* in Fig.2). The other part is the time of radiation propagation from position of the electron $\vec{r}(t_e(x_s))$ to the point at the observation screen $\vec{X}_s = \{x_s,0,D\}$, that is the quantity $\frac{1}{c}\left|\vec{X}_s - \vec{r}(t_e(x_s))\right|$.

At some moment t the electron's position was $\vec{r}(t)$ and its velocity was pointed to the observer with the coordinates $\{x_s(t),0,D\}$. It can easily be shown from Fig. 2 that:

$$x_s(t) = r_x(t) + (D - r_z(t))\cdot tg\varphi\,, \tag{8}$$

where $\varphi = \Omega t$.

It follows from Eq. (6) and Eq. (8) that:

$$x_s(t) = R + D\cdot tg(\Omega t) - \frac{R}{\cos(\Omega t)}\,, \tag{9}$$

The case $\beta_z(t) > 0$ (i.e. $\cos(\Omega t) > 0$) is of interest for our analysis. By using the relation $1 + tg^2(\varphi) = 1/\cos^2(\varphi)$, we can get from Eq. (9):

$$\left(D^2 - R^2\right)tg^2(\Omega t) + 2D\left(R - x_s(t)\right)tg(\Omega t) + x_s^2(t) - 2Rx_s(t) = 0\,. \tag{10}$$

This equation is quadratic in terms of $tg(\Omega t)$ with the solution:

$$tg(\Omega t_e(x_s)) = \frac{R\sqrt{(R - x_s)^2 + D^2 - R^2} - D(R - x_s)}{D^2 - R^2}\,. \tag{11}$$

This is precisely the solution of the two solutions of the quadratic equation (10) which gives $t_e(x_s = 0) = 0$. Here we consider the quantity x_s as an independent variable. Thus, $t_e(x_s)$ is the moment when the electron, having the position $\vec{r}(t_e(x_s))$, points to the observer with the coordinates $\{x_s, 0, D\}$. As a result, we have the following expression for the arriving time $\tau(x_s)$ of synchrotron radiation pulse:

$$\tau(x_s) = t_e(x_s) + \frac{1}{c}\left|\vec{X}_s - \vec{r}(t_e(x_s))\right| . \tag{12}$$

It is convenient to define the function $\varphi(x_s)$:

$$\varphi(x_s) = \arctan\left(\frac{R\sqrt{(R-x_s)^2 + D^2 - R^2} - D(R-x_s)}{D^2 - R^2}\right), \tag{13}$$

with $\varphi(x_s = 0) = 0$ and $t_e(x_s) = \frac{1}{\Omega}\varphi(x_s) = \frac{R}{c\beta}\varphi(x_s)$. In essence the function $\varphi(x_s)$ is the angle $\varphi = \Omega t$, at which the electron velocity $\vec{\beta}(t)$ points to the observer $\vec{X}_s = \{x_s, 0, D\}$, see Fig. 2.

As a result, we will get the following expression for the arriving time $\tau(x_s)$:

$$\tau(x_s) = \frac{R}{c\beta}\varphi(x_s) + \frac{1}{c}\sqrt{\left(x_s - R + R\cos(\varphi(x_s))\right)^2 + \left(D - R\sin(\varphi(x_s))\right)^2} . \tag{14}$$

Looking ahead, we note that the value of $2\pi c\tau(x_s)/\lambda$ is a phase of the radiation with the wavelength λ.

The x_s-dependence of the function $c\Delta\tau(x_s) = c\left(\tau(x_s) - \tau(0)\right)$ is shown in Fig. 3a. The parameters of Siberia-2 storage ring were used for this simulation: electron beam energy 2.5 GeV (electron reduced energy is equal to γ =4892), electron orbit radius R =4905.4 mm, synchrotron radiation critical energy 7.2 keV (Korchuganov et al., 2005; Korchuganov & Smolyakov, 2009). The distance of the observation plane from the emission point was taken to be D = 20000 mm.

The quadratic behaviour of retardation $c\Delta\tau(x_s)$ suggests that the synchrotron radiation phase distribution is very close to that of an immobile point source. Closer examination of the derived above expressions shows that the correspondent equivalent point source, which produces the similar phase distribution, should be placed at the point with coordinates $\left\{\frac{-R}{2\gamma^2}, 0, 0\right\}$. Practically the value $\frac{-R}{2\gamma^2}$ is very small; in our case it is equal to 10^{-4} mm. The front position for this point source is described by the following expression:

$$\Delta d(x_s) = \sqrt{\left(x_s + R/(2\gamma^2)\right)^2 + D^2} - \sqrt{\left(R/(2\gamma^2)\right)^2 + D^2} . \tag{15}$$

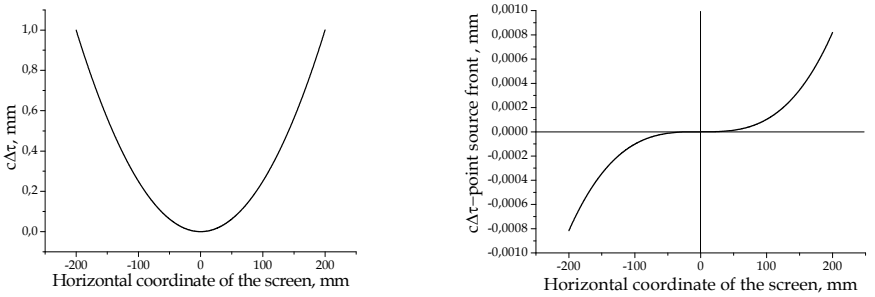

a b

Fig. 3. (a) Synchrotron radiation retardation $c\Delta\tau(x_s)$ versus observer horizontal position x_s. (b) Difference in positions between synchrotron radiation front and point source front.

The difference between the synchrotron radiation front position $c\Delta\tau(x_s)$ and the point source front position $\Delta d(x_s)$ is shown in Fig. 3b. It should be pointed out that this difference is small, less to 10^{-3} mm at the horizontal aperture boundaries ± 200 mm in our example. It means that the synchrotron radiation phase can be considered at zero approximation as the spherically symmetric phase of the correspondent immobile point source. Expanding Eqs. (13) – (15) in powers of x_s we get the following approximation for the difference in front positions of synchrotron radiation and point source front (Fig. 3b):

$$c\Delta\tau(x_s) - \Delta d(x_s) \cong \left(Rx_s^3\right) \Big/ \left(6D^3\right). \tag{16}$$

It describes the curve in Fig. 3b with a very good accuracy. Though this term is cubic in x_s and is very small at first glance, it plays an important part in synchrotron radiation imaging, as we will see below.

Finally we will give another well-known example, which on closer examination also shows the phase distribution of synchrotron radiation. Let an electron moves anticlockwise along the circle trajectory $\vec{r}(t)$, see Fig. 4. The radiation pulse (the maximum of the generated electric field) moves along the velocity vector $\vec{\beta}(t)$. At time τ it will reach the point $\vec{X}(\tau) = \vec{r}(t) + \frac{\vec{\beta}(t)}{\beta} c(\tau - t)$. Let us substitute Eqs. (6) and (7) into this relation, fix an observation point in time τ and consider the set of points in time t when the radiation was emitted: $t < \tau$. We will get the simultaneous distribution of the radiation pulses in the space, the well-known spiral radiation pattern, see Fig. 4. Some comments to this pattern can be found in (Jackson, 1999). The numbers of computed diagrams of electric field lines of radiating electron are published by (Tsien, 1972), see also (Shintake, 2003).

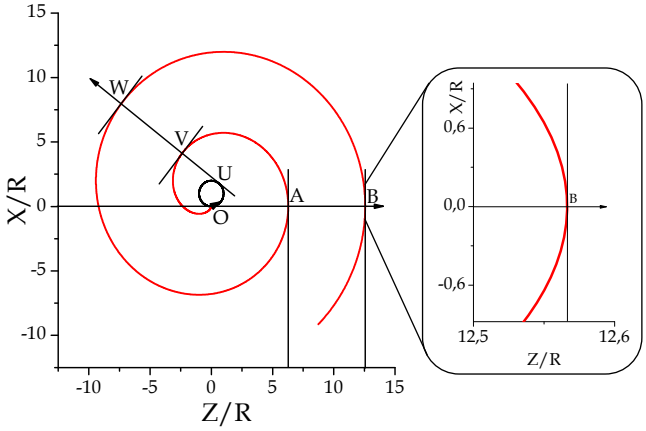

Fig. 4. The left side: space distribution of synchrotron radiation in the median plane. Small black circle is the electron trajectory which rotates anticlockwise. The right side: a magnified element of the spiral pattern.

Let us draw a line along the electron velocity $\vec{\beta}(t)$ tangentially to the electron trajectory (the direction of the radiation propagation) and consider the observation screen transversal to this line as it is shown on Fig.4, left side. The radiation at the point A was emitted at the point O one electron turn ago and the radiation at the point B was emitted two electron turns ago. The radiation at the point A moves along the line $O-A-B$ towards the point B. Similarly, we can say about the radiation which is generated at the point U and propagates along the line $U-V-W$. What is important for us in this picture is the fact that the spiral pattern is tangent to the screen and locally has the behaviour of quadratic function relative to horizontal (X) coordinates as it is shown at the right side of Fig.4. So, this spiral pattern also displays the phase distribution similar to the point source phase behaviour.

3. Synchrotron radiation phase distribution

In this section we will derive the exact expressions for synchrotron radiation phase. Let us consider an electron moving along trajectory $\vec{r}(t)$ with reduced energy $\gamma >> 1$. Electric field in the emitted wave which is observed at the point $\vec{X} = \{x, y, D\}$ and time τ is equal to:

$$\vec{E}(\tau,\vec{X}) = \frac{e}{c\left|\vec{X}-\vec{r}(t)\right|}\frac{[\vec{n}\times[(\vec{n}-\vec{\beta}(t))\times\dot{\vec{\beta}}(t)]]}{(1-\vec{n}\cdot\vec{\beta}(t))^3} + \frac{e}{\left|\vec{X}-\vec{r}(t)\right|^2}\frac{(\vec{n}-\vec{\beta}(t))(1-\beta^2(t))}{(1-\vec{n}\cdot\vec{\beta}(t))^3}, \qquad (17)$$

where c is the speed of light, e is the electron charge, $\vec{\beta}$ is its reduced velocity, $\gamma = \frac{1}{\sqrt{1-\beta^2}}$, $\vec{n} = \frac{\vec{X}-\vec{r}(t)}{\left|\vec{X}-\vec{r}(t)\right|}$, and t is emission time:

$$\tau = t + \frac{1}{c}\left|\vec{X} - \vec{r}(t)\right| . \tag{18}$$

The radiation spectrum with wavelength λ is defined by the Fourier transform:

$$\tilde{\vec{E}}(\lambda, \vec{X}) = \int_{-\infty}^{\infty} \exp(i\frac{2\pi c}{\lambda}\tau)\vec{E}(\tau, \vec{X})d\tau \, , \tag{19}$$

The unit vectors of polarization $\vec{q}_\sigma$ and $\vec{q}_\pi$ are directed transversally to the radiation propagation and describe horizontally and vertically polarized radiation correspondently. The number of photons per unit time per unit area per unit relative spectral interval emitted by an electron beam with current I is equal to:

$$\frac{dN_{\sigma,\pi}}{d\tau\, ds(d\lambda/\lambda)} = \frac{c}{4\pi^2\hbar}\frac{I}{e}\left|\left(\vec{q}_{\sigma,\pi}\cdot\tilde{\vec{E}}(\lambda, \vec{X})\right)\right|^2 \tag{20}$$

It can easily be shown by the direct differentiation of Eq. (18) that:

$$\frac{\partial\tau(t)}{\partial t} = 1 - (\vec{n}\cdot\vec{\beta}(t)) . \tag{21}$$

Using Eq. (21) we can write: $\tau(t) = \tau(T) + \int_T^t (1 - \vec{n}\cdot\vec{\beta}(t'))dt'$, or:

$$\tau(t) = T + \frac{1}{c}\left|\vec{X} - \vec{r}(T)\right| + f(T, t) \, , \tag{22}$$

where

$$f(T, t) = \int_T^t (1 - \vec{n}\cdot\vec{\beta}(t'))dt' . \tag{23}$$

Here T is an arbitrary quantity to be defined below. It is important to keep in mind that T does not depend on time t .

Substituting Eqs. (17) and (18) into Eq. (19) and changing the integration from the independent variable τ to the variable t with the help of Eq. (21), we get:

$$\tilde{\vec{E}}(\lambda, \vec{X}) = \exp\left(i\Phi(T, \vec{X})\right)\tilde{\vec{E}}_0(\lambda, \vec{X}) \, , \tag{24}$$

where

$$\Phi(T, \vec{X}) = \frac{2\pi}{\lambda}\left\{cT + \left|\vec{X} - \vec{r}(T)\right|\right\} \tag{25}$$

$$\tilde{\vec{E}}_0(\lambda, \vec{X}) = \frac{e}{c}\int_{-\infty}^{\infty} \exp\left(i\frac{2\pi c}{\lambda}f(T, t)\right)\left\{\frac{[\vec{n}\times[(\vec{n}-\vec{\beta})\times\dot{\vec{\beta}}]]}{\left|\vec{X} - \vec{r}(t)\right|(1-\vec{n}\cdot\vec{\beta})^2} + \frac{c}{\left|\vec{X} - \vec{r}(t)\right|^2}\frac{(\vec{n}-\vec{\beta})(1-\beta^2)}{(1-\vec{n}\cdot\vec{\beta})^2}\right\}dt \tag{26}$$

Once the radiation intensity is calculated, the Eq. (24) should be substituted into Eq. (20) and the phase $\Phi(T,\vec{X})$ is of no concern. But the applications of optical elements generate a need for the radiation phase $\Phi(T,\vec{X})$ accurate calculations.

It is a matter of direct verification to prove the following exact relation:

$$\frac{[\vec{n}\times[(\vec{n}-\vec{\beta})\times\dot{\vec{\beta}}]]}{\left|\vec{X}-\vec{r}(t)\right|(1-\vec{n}\cdot\vec{\beta})^2}+\frac{c}{\left|\vec{X}-\vec{r}(t)\right|^2}\frac{(\vec{n}-\vec{\beta})(1-\beta^2)}{(1-\vec{n}\cdot\vec{\beta})^2}=\frac{d}{dt}\left\{\frac{\vec{n}-\vec{\beta}}{\left|\vec{X}-\vec{r}(t)\right|(1-\vec{n}\cdot\vec{\beta})}\right\}+\frac{c\vec{n}}{\left|\vec{X}-\vec{r}(t)\right|^2} \quad (27)$$

Substituting Eq. (27) into Eq. (26) and integrating by parts with using Eq. (23), we get:

$$\tilde{\vec{E}}_0(\lambda,\vec{X})=-i\frac{2\pi e}{\lambda}\int_{-\infty}^{\infty}\exp\left(i\frac{2\pi c}{\lambda}f(T,t)\right)\left\{\vec{n}(t)\left(1+\frac{i\lambda}{2\pi\left|\vec{X}-\vec{r}(t)\right|}\right)-\vec{\beta}(t)\right\}\frac{dt}{\left|\vec{X}-\vec{r}(t)\right|} \quad (28)$$

It should be noted that so far the exact formulas (17) - (28) were used and no approximations were employed. Particular attention should be paid to the phase as its scale of variation is very small, the phase changes by 2π along the radiation wavelength. Furthermore, we will derive the exact expression for synchrotron radiation phase distribution which is given by Eq. (25). At the same time we will apply the standard far-field approximation in the radiation amplitudes calculations, see Eq. (28).

We detect the radiation at the point $\vec{X}=\{x,y,D\}$, where D is considered to be much greater than the size of the emission region. Then we can write $\left|\vec{X}-\vec{r}(t)\right|=D$, $n_x=x/D$, $n_y=y/D$ and certainly we can neglect by the small term $i\lambda/\left(2\pi\left|\vec{X}-\vec{r}(t)\right|\right)$ in Eq. (28). The polarization vectors are

$$\begin{aligned}\vec{q}_\sigma&=[\vec{j}\times\vec{n}]/\left|[\vec{j}\times\vec{n}]\right|,\\ \vec{q}_\pi&=[\vec{n}\times\vec{q}_\sigma],\end{aligned} \quad (29)$$

where $\vec{j}$ is the unit vector along vertical Y-axis. Let us consider the radiation at small observation angles: $\left|n_{x,y}\right|<<1$ so that $n_z=\sqrt{1-n_x^2-n_y^2}$ is approximately equal to:

$$n_z=1-0.5\cdot(n_x^2+n_y^2). \quad (30)$$

Similarly, the expansion for $\beta_z(t)=\sqrt{\beta^2-\beta_x^2(t)}$ is equal to:

$$\beta_z(t)=1-0.5\cdot(\gamma^{-2}+\beta_x^2(t)). \quad (31)$$

It can be easily derived from Eq. (30) and Eq. (31) that:

$$1-(\vec{n}\cdot\vec{\beta})=0.5\cdot\left(\gamma^{-2}+(n_x-\beta_x)^2+n_y^2\right). \tag{32}$$

Then we obtain from Eq. (28):

$$\widetilde{E}_{0\sigma,\pi}(\lambda,\vec{X})=-i\frac{2\pi e}{\lambda D}\int_{-\infty}^{\infty}\exp\left(i\frac{2\pi c}{\lambda}f(T,t)\right)\left(\vec{n}-\vec{\beta}(t)\right)_{x,y}dt \tag{33}$$

and

$$f(T,t)=\frac{1}{2\gamma^2}\int_T^t\left(1+\gamma^2\left(n_x-\beta_x(t')\right)^2+\gamma^2 n_y^2\right)dt'. \tag{34}$$

Usually, calculating synchrotron radiation intensity, the observation point is chosen in such a way that $n_x=0$ thus substantially simplifying the resultant calculations. It is possible for the amplitudes calculations because they are axially uniform and depends on vertical angle only. In this case we obtain $\left(\vec{q}_\sigma\cdot\vec{\widetilde{E}}(\lambda,\vec{X})\right)$ as a purely real function and $\left(\vec{q}_\pi\cdot\vec{\widetilde{E}}(\lambda,\vec{X})\right)$ as a purely imaginary function. But this simplification is not applicable when calculating the phase distribution of synchrotron radiation and we need to apply more accurate calculating procedure.

Now we determine the parameter T by making it equal to $t_e(x)$, where x is the horizontal coordinate of the observation point $\vec{X}=\{x,y,D\}$ and the function $t_e(x)$ is given by Eq. (11). By using the relation $tg\varphi=\dfrac{\beta_x(t)}{\beta_z(t)}$, see Eqs. (7), we get from Eq. (8):

$$\frac{x-r_x(t_e(x))}{D-r_z(t_e(x))}=\frac{n_x}{n_z}=\frac{\beta_x(t_e(x))}{\beta_z(t_e(x))}. \tag{35}$$

Saving the linear terms of Eq. (35), which is to say that $n_z\cong 1$ and $\beta_z\cong 1$, we get: $\beta_x(t_e(x))=n_x=\dfrac{x}{D}$ and hence in the frame of linear approximation:

$\beta_x(t)=\beta\sin(\Omega t_e(x))\cos(\Omega\Delta t)+\beta\cos(\Omega t_e(x))\sin(\Omega\Delta t)\cong n_x+\Omega\Delta t$, where $t=t_e(x)+\Delta t$.

Substituting this relation into Eq. (34) and denoting $\chi=\gamma\Omega\Delta t$, where $\Omega=\beta c/R$, we obtain:

$$f(T=t_e(x),t)=\frac{R}{2\gamma^3 c}\left\{\left(1+\gamma^2 n_y^2\right)\chi+\frac{1}{3}\chi^3\right\}. \tag{36}$$

Using Eq. (36), we can easily derive from Eq. (33) the well-known expressions for synchrotron radiation fields:

$$\widetilde{E}_{0\sigma}(\lambda,\vec{X})=\frac{4\pi e\gamma}{Dc}\sqrt{\Lambda}Ai'\left(\Lambda\left(1+\gamma^2 n_y^2\right)\right), \tag{37}$$

$$\widetilde{E}_{0\pi}(\lambda,\vec{X}) = -i\frac{4\pi e\gamma^2}{Dc}\Lambda n_y Ai\left(\Lambda\left(1+\gamma^2 n_y^2\right)\right) \tag{38}$$

where $\Lambda = \left(\frac{\pi R}{\lambda\gamma^3}\right)^{2/3} = \left(\frac{3\lambda_c}{4\lambda}\right)^{2/3}$, $\lambda_c = \frac{4\pi R}{3\gamma^3}$ is the synchrotron radiation critical wavelength, $Ai(x)$ and $Ai'(x)$ are the Airy function and its derivative.

We have obtained standard formulas, describing the synchrotron radiation amplitudes $\widetilde{E}_{0\sigma}$ and $\widetilde{E}_{0\pi}$ in the far-field approximation. The phases of the amplitudes $\widetilde{E}_{0\sigma}$ and $\widetilde{E}_{0\pi}$ are constant (independent of the observation point position), so the phase dependence of the synchrotron radiation is described by the function $\Phi(T = t_e(x),\vec{X})$, see Eq. (25):

$$\Phi(\vec{X}) \equiv \Phi(T = t_e(x),\vec{X}) = \frac{2\pi c}{\lambda}\left\{t_e(x) + \frac{1}{c}\left|\vec{X} - \vec{r}(t_e(x))\right|\right\} \tag{39}$$

Notice that $t_e(x)$ is the moment when the electron, having the position $\vec{r}(t_e(x))$, points to the observer with the coordinates $\{x,0,D\}$. The second term $\frac{1}{c}\left|\vec{X} - \vec{r}(t_e(x))\right|$ is the time interval required for the light passing from the position of the electron $\vec{r}(t_e(x))$ to the observer position $\vec{X} = \{x,y,D\}$. Thus, we have obtained a physically reasonable result that the synchrotron radiation phase is proportional to the arrival time of the maximum of function $E_\sigma(\tau,\vec{X})$: the arrival time is equal to $\lambda\Phi(\vec{X})/(2\pi c)$.

Let us determine the following variables: $\rho = \frac{R}{D}$, $\theta_x = \frac{x}{D}$, $\theta_y = \frac{y}{D}$ and a function $\delta(\theta_x)$:

$$\delta(\theta_x) = \arctan\frac{\rho\sqrt{(\rho-\theta_x)^2 + 1 - \rho^2} - (\rho - \theta_x)}{1-\rho^2}. \tag{40}$$

Notice that $\delta(\theta_x = 0) = 0$. Then the phase distribution of synchrotron radiation is described by the following exact expression:

$$\Phi(\vec{X}) = \frac{2\pi D}{\beta\lambda}\left\{\rho\delta + \beta\sqrt{(1-\rho\sin\delta)^2 + (\theta_x + \rho\cos\delta - \rho)^2 + \theta_y^2}\right\}. \tag{41}$$

It is worth noting that we have obtained, as a result, the exact analytic expression involving only elementary functions. It is important to outline also that the phase difference, rather than the phase value $\Phi(\vec{X})$, has a physical sense. In other words, the phase is defined up to a constant value identical for all the points of the optical device entrance window.

4. Synchrotron radiation regarded as a point-source radiation

Consider now the phase $\Phi(\vec{X})$ at the observation point $\vec{X} = \{x,y,D\}$, where $|x| << D$, $|y| << D$. Analysis shows that the function $\Phi(\vec{X})$ has a minimum in the vicinity of the point

$\{0,0,D\}$. Let us expand this phase in a power series with respect to the small transverse angles $\theta_x = \frac{x}{D}$ and $\theta_y = \frac{y}{D}$ up to the third power inclusive. This expansion has the form:

$$\Phi(\vec{X}) = \Phi_0 + \Phi_2(\vec{X}) + \Phi_3(\vec{X}), \tag{42}$$

$$\Phi_0 = \frac{2\pi D}{\lambda}\left\{1 - R^2/(8D^2\gamma^4)\right\}, \tag{43}$$

$$\Phi_2(\vec{X}) = \frac{\pi D}{\lambda}\left\{\left(\theta_x + \frac{\rho}{2\gamma^2}\right)^2 + \theta_y^2\right\}, \tag{44}$$

$$\Phi_3(\vec{X}) = \frac{\pi R}{\lambda}\left\{\frac{1}{3}\theta_x^3 + \theta_x\theta_y^2\right\}. \tag{45}$$

If both angles θ_x and θ_y are sufficiently small, one can neglect the term $\Phi_3(\vec{X})$, which is of the third order of smallness. The size of the corresponding region can be evaluated from condition $\Phi_3(\vec{X}) < 0.5\pi$. As a result, one finds that the term $\Phi_3(\vec{X})$ can be neglected if:

$$\left|\theta_{x,y}\right| < \frac{1}{\gamma}\sqrt[3]{\frac{\lambda}{\lambda_c}}. \tag{46}$$

In this case $\Phi(\vec{X}) = \Phi_2(\vec{X})$ and the distribution of the synchrotron radiation phases coincides with the phase distribution of an immobile point source located at the point $\left\{-\frac{R}{2\gamma^2},0,0\right\}$. The quantity $\frac{R}{2\gamma^2}$ usually is very small and can be neglected. Then it is seen from Eq. (44) that the equivalent immobile point source is located at the origin of the coordinates. In this case the synchrotron radiation properties are rather well understood. The spatial distributions of the synchrotron radiation amplitudes are described by Eqs. (37) and (38). The synchrotron radiation phase distribution inside the angle limited by Eqs. (46) coincides with that of an equivalent spherical wave propagating from the origin of the coordinates and is described by Eq. (44). For the Siberia-2 storage ring (γ =4892, λ_c =0.175 nm, λ =6000 nm) the region given by Eq. (46) is rather large: $\left|\theta_{x,y}\right| < 6.6$ mrad. Any decrease in the radiation wavelength reduces the size of this region.

All the above stated concerned a single relativistic electron moving along the circular trajectory with zero initial conditions see Eqs. (6) and (7) and Fig. 5. This electron passed through the origin of the coordinates, where its velocity was directed along the Z-axis. The immobile point source, which is equivalent in phase distribution to the synchrotron radiation generated by this electron, is at the origin of the coordinates. However, in practice the electron beam has always some spread in both positions and angles. It is clear that for electrons with different orbits the locations of the equivalent immobile point sources would

also be different. The explicit calculation of the position of the equivalent point source for an arbitrary electron involves rather cumbersome formulas and is beyond the scope of this chapter. However, for an electron with a trajectory lying in the storage ring median plane, the solution is reasonably simple.

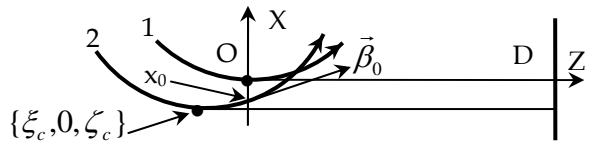

Fig. 5. Equivalent immobile point sources positions sketch: the point source $\{-R/(2\gamma^2), 0, 0\}$ for the electron 1 with zero initial conditions and the point source $\{\xi_c, 0, \zeta_c\}$ for the electron 2 with nonzero initial conditions.

Let us consider now an electron moving along a circular trajectory which lies in the XOZ-plane and intersects the X-axis at some point x_0 so that the electron initial position is $\{x_0, 0, 0\}$. Let the vector $\{\beta_{x0}, 0, \beta_{z0}\}$ be the reduced velocity of the electron at this initial point and β_{x0} be small. According to the analysis, the phase distribution of the synchrotron radiation in this case coincides with the phase distribution of an equivalent spherical wave outgoing from a point source with the coordinates $\{\xi_c, 0, \zeta_c\}$, where:

$$\xi_c = x_0 - \frac{R}{2\gamma^2} - 0.5R\beta_{x0}^2, \zeta_c = -R\beta_{x0}. \tag{47}$$

Up to $R/(2\gamma^2)$, this point source lies on the electron orbit. Namely, it is the point of tangency of a normal to the screen with the electron circular trajectory, see Fig.5. Notice that the transverse (X) coordinate ξ_c depends mainly on the electron initial position x_0, while its longitudinal (Z) coordinate ζ_c is determined by the electron initial angle β_{x0}.

Let us consider a relativistic beam, in which all the electron trajectories lie in the XOZ-plane (zero vertical emittance condition). Nevertheless, these electrons are spread over horizontal positions and angles. In the vicinity of the optical device window (as defined by Eq. (46)) the synchrotron radiation of such a beam can be regarded as a radiation from a set of immobile point sources, whose coordinates are defined by Eqs. (47). The phases of the synchrotron radiation emitted by each of the electrons coincide with the phases of the radiation emitted by the corresponding immobile point sources. However, according to Eqs. (37) and (38), the radiation amplitudes of the immobile point sources are modulated in the vertical direction. This approach permits us to substitute of a determination of a pattern produced by the distributed immobile point sources for the calculation of the image created by the synchrotron radiation. The solution of this problem has been comprehensively examined by the wave optics (Born & Wolf, 1986). It is significant that the length along Z-axis of this immobile point sources distribution is determined by the electron beam angular spread rather than the orbit curvature and a focusing lens aperture as implied in the geometrical optics approach (Hofmann & Meot, 1982).

It should be said in closing that the term $\Phi_3(\vec{X})$, which was outside our analysis here, plays an important role in synchrotron radiation optics, determining its self-aberration effect.

5. Focusing of synchrotron radiation

Let us consider the standard experimental layout for synchrotron radiation imaging shown in Fig. 6. For simplicity sake the geometry with an ideal refractive lens is considered. The distance between the origin of coordinates and lens is equal to D, the distance from the lens to the observation screen is equal to L.

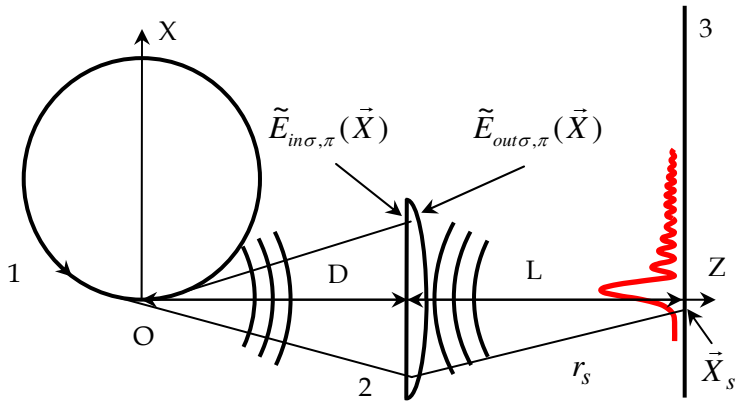

Fig. 6. Synchrotron radiation imaging experiment geometry: 1 – electron trajectory; 2 – lens, 3 – observation screen.

The ideal lens with focal length f does not change the synchrotron radiation amplitudes but adds an extra shift in the radiation phase distribution:

$$\vec{E}_{out}(x,y,z=D)=\vec{E}_{in}(x,y,z=D)\cdot\exp\left(-i\pi(x^2+y^2)/(\lambda f)\right). \tag{48}$$

Here $\vec{E}_{in}(x,y,z=D)=\exp\left(i\Phi(\vec{X})\right)\tilde{\tilde{E}}_0(\lambda,\vec{X})$ is the synchrotron radiation field. Its amplitudes $\tilde{\tilde{E}}_0$ are given by Eqs. (37) and (38) and the phase $\Phi(\vec{X})=\Phi_2(\vec{X})+\Phi_3(\vec{X})$ is given by Eqs. (42) – (45). Notice that the cubic term $\Phi_3(\vec{X})$ will also be taken here into account.

The radiation field at the point $\vec{X}_s=\{x_s,y_s,z_s=D+L\}$ of the observation screen can be found by applying the Kirchhoff integral theorem (Born & Wolf, 1986):

$$\vec{E}(x_s,y_s,z_s)=\frac{-i}{\lambda}\int_A\vec{E}_{out}(x,y,z=D)\frac{\exp(ikr_s)}{r_s}dxdy\ , \tag{49}$$

where $r_s = \sqrt{(x-x_s)^2 + (y-y_s)^2 + L^2} \cong L + \frac{(x-x_s)^2 + (y-y_s)^2}{2L}$ is the distance of the lens element $dxdy$ from the observer $\vec{X}_s = \{x_s, y_s, z_s = D + L\}$ and A is the lens aperture, which is assumed rectangular in shape here. Calculating numerically the Kirchhoff integral (49), we can find with Eq. (20) the intensity distribution of the focused synchrotron radiation.

The computed images of horizontally and vertically polarized synchrotron radiation are shown in Fig. 7. The simulations were performed at the following conditions: orbit bending radius 4905.4 mm; electron beam energy of 2.5 GeV; beam current 0.1 A; beam emittance is zero (one-electron approximation); lens focal length 5 m; distance from tangential source point to the lens 10 m; distance from the lens to the observation screen 10 m; horizontal and vertical sizes of the lens 600 mm (angular aperture 60 mrad); radiation wavelength 6000 nm. The lens focuses the synchrotron radiation emitted into all vertical angles, see Fig. 8.

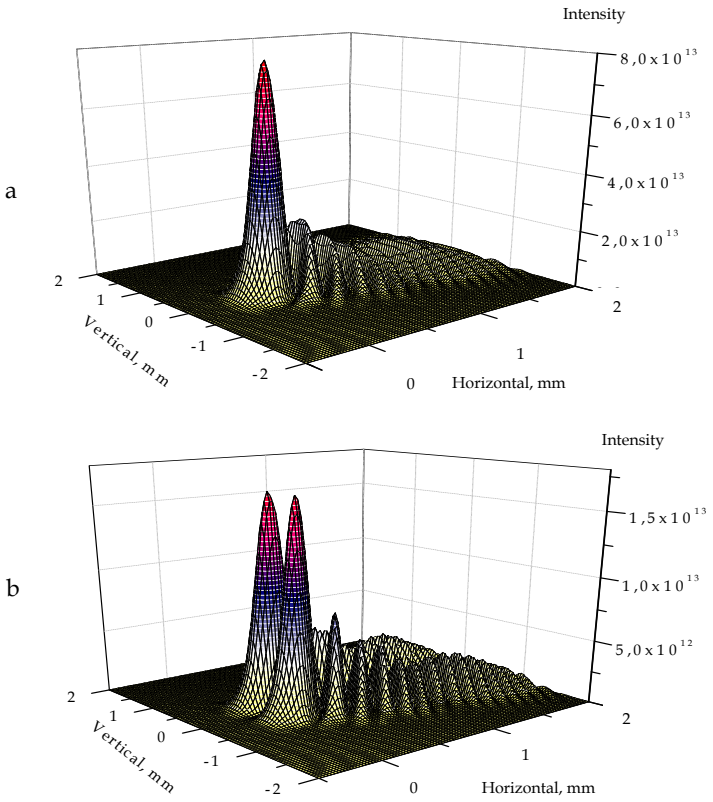

Fig. 7. Intensity distributions of the focused synchrotron radiation: a – horizontally (σ) polarized component of radiation; b – vertically (π) polarized component of radiation. Intensity distributions are given in photons/s/mm²/(0.1%bandwidth).

It is significant that the intensity of focused vertically polarized synchrotron radiation is equal to zero in the electron orbit plane ($y=0$), see Fig. 7b. This is a result of the anti-symmetry of the vertically polarized electric field with respect to the electron orbit plane, see Fig. 8 and Eq. (38): $\widetilde{E}_{0\pi}(\lambda,\vec{X})$ is proportional to $n_y = y/D$. Thus two rays with the opposite signs of n_y and respectively with the opposite electric field directions, when focused to the point $\{x_s, 0, z_s = D+L\}$, will cancel each other.

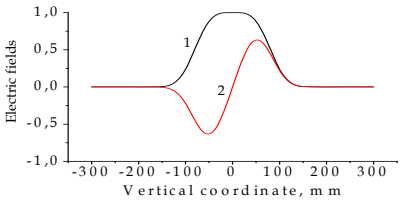

Fig. 8. Vertical distributions of synchrotron radiation electric fields $\widetilde{E}_{0\sigma,\pi}(\lambda,\vec{X})$ on the lens surface: 1 – horizontally polarized radiation, 2 – vertically polarized radiation.

At large horizontal aperture of the lens (600 mm) the cubic term $\Phi_3(\vec{X})$ in the radiation phase manifests itself as additional asymmetric fringes in the radiation image (self-aberration effect). Real electron beam emittance will smooth out these fringes. Nevertheless, such asymmetry was observed in 100 - 20000 cm^{-1} spectral range at BL43IR infrared beamline of Spring-8 (Ikemoto et al., 2003), see Fig. 9.

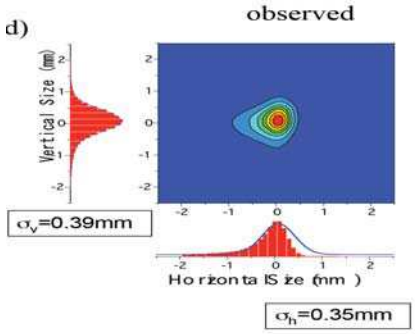

Fig. 9. Experimentally observed at Spring-8 image of the electron beam.
(Published with the kind permission of Prof. T. Nanba)

Let us consider now the influence of the lens horizontal aperture on the synchrotron radiation imaging. It follows from Eq. (46) that the natural scale for the angular aperture is

$$\Delta\theta_{SR} = \frac{2}{\gamma}\cdot\sqrt[3]{\frac{\lambda}{\lambda_c}} \cong 1.24\cdot\sqrt[3]{\frac{\lambda}{R}}\,. \tag{50}$$

For the Siberia-2 storage ring with the orbit bending radius $R = 4905.4$ mm and for $\lambda = 6000$ nm this value is equal to $\Delta\theta_{SR} = 13.3$ mrad. Fig. 10 shows the computed radiation intensity distributions in the electron orbit plane $y = 0$. The simulations were performed under the same conditions as above except for the lens horizontal size. The lens horizontal aperture $2l_x$ was taken equal to 66 mm, 132 mm, 264 mm and 528 mm, that is the lens horizontal angular aperture $\theta_{lens} = 2l_x/D$ is equal to $0.5\Delta\theta_{SR}$, $\Delta\theta_{SR}$, $2\Delta\theta_{SR}$ and $4\Delta\theta_{SR}$ respectively.

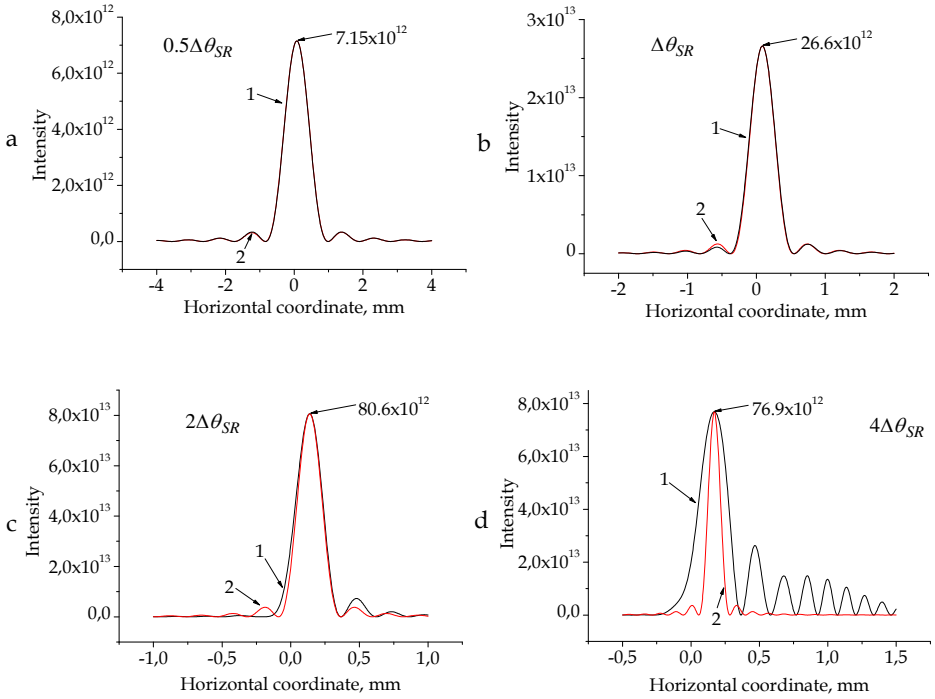

Fig. 10. Intensity distributions (photons/s/mm²/(0.1%bandwidth)) in the median plane of the focused synchrotron radiation for different horizontal angular aperture θ_{lens} of the lens: a - $\theta_{lens} = 0.5\Delta\theta_{SR}$, b - $\theta_{lens} = \Delta\theta_{SR}$, c - $\theta_{lens} = 2\Delta\theta_{SR}$ and d - $\theta_{lens} = 4\Delta\theta_{SR}$.
Curve 1 - focused synchrotron radiation, curve 2 – approximation by $(\sin(\xi)/\xi)^2$, see Eq. (5).

From Fig.10 we notice that the function $(\sin(\xi_s)/\xi_s)^2$ with $\xi_s = \frac{2\pi l_x}{\lambda L} x_s$, when normalised and horizontally shifted, adequately describes the horizontal profiles of the focused synchrotron radiation up to $\theta_{lens} = 2\Delta\theta_{SR}$. But at large horizontal aperture of the lens, the self-aberration property of synchrotron radiation changes dramatically the radiation image characteristics. For the case of point source radiation its intensity at the focused spot center varies with the square of the lens horizontal aperture, see the end of the section 2.1. This is also true for synchrotron radiation focusing by relatively small lens; at small θ_{lens} its value

doubling tends to increase the maximum of intensity by a factor of four approximately. But the increasing of the lens horizontal aperture from $\theta_{lens} = 2\Delta\theta_{SR}$ to $\theta_{lens} = 4\Delta\theta_{SR}$ implies a decrease in the maximum of the focused synchrotron radiation intensity, see Fig 10.

Such kind of problems, which are caused by the self-aberration effect of synchrotron radiation (the term $\Phi_3(\vec{X})$), can be neutralized by using of the so-called "magic mirror". The idea how to bring a segment of circular orbit to an isochronous focus and profile of such mirror in the orbit plane was presented in (Lopez-Delgado & Szwarc, 1976). The expansion of formula for "magic mirror" to include the vertical direction was made in (S. Kimura et al., 2001). The "magic mirror" for synchrotron radiation is similar to the ideal lens for a point source radiation since it compensates the aberrations caused by the term $\Phi_3(\vec{X})$ in design. It is employed at some infrared beamlines (H. Kimura et al., 2001; S. Kimura et al., 2006).

6. Conclusion

The analysis of wave optical properties of synchrotron radiation given in this chapter shows their unconventionality. On the one hand, in the zero-order approximation the phases of the synchrotron radiation emitted by each of the electrons coincide with the phases of the radiation emitted by the corresponding immobile point sources. That is why standard optical equipment works well with synchrotron radiation paraxial beams. On the other hand, synchrotron radiation has the property of self-aberration. To improve beamline performance, the specialized optical elements, such as the "magic mirror", should be used in the beamline optical system. The use of the exact formula for the phase distribution of synchrotron radiation provides a way of developing new optical elements which are optimized for synchrotron radiation utilization.

7. References

Andersson, A.; Schlott, V.; Rohrer, M.; Streun, A. & Chubar, O. (2006). Electron beam profile measurements with visible and X-Ray synchrotron radiation at the Swiss Light Source, *Proceedings of the tenth European Particle Accelerator Conference (EPAC'06)*, pp. 1223-1225, ISBN 92-9083-278-9, Edinburgh, Scotland, June 26-30, 2006

Andersson, A. & Tagger, J. (1995). Beam profile measurements at MAX. *Nuclear Instruments and Methods in Physics Research A*, Vol.364, No.1, (September 1995), pp. 4-12, ISSN 0168-9002

Arp, U. (2001). Diffraction and depths-of-field effects in electron beam imaging at SURF III. *Nuclear Instruments and Methods in Physics Research A*, Vol.462, No.3, (April 2001), pp. 568-575, ISSN 0168-9002

Artemiev, N. A.; Chubar, O. V. & Valentinov, A. G. (1996). Electron beam diagnostics with visible synchrotron light on Siberia-1 ring, *Proceedings of the fifth European Particle Accelerator Conference (EPAC'96)*, pp. 340-342, ISBN 978-0-7503-0387-3, Barcelona, Spain, June 10-14, 1996

Bahrdt, J. (1997). Wave-front propagation: design code for synchrotron radiation beam lines. *Applied Optics,* Vol.36, No.19, (July 1997), pp. 4367-4381, ISSN: 1559-128X

Bahrdt, J. (2007). Wavefront tracking within the stationary phase approximation. *Physical Review Special Topics – Accelerators and Beams*, Vol.10, No.6, (June, 2007), pp. 060701-1 – 060701-15, ISSN 1098-4402

Bocci, A.; Clozza, A.; Drago, A.; Grilli, A.; Marcelli, A.; Piccinini, M.; Raco, A.; Sorchetti, R.; Gambicorti, L.; De Sio, A.; Pace, E. & Piotrowski, J. (2008). Beam diagnostics with IR light emitted by positrons at DAFNE, *Proceedings of the eleventh European Particle Accelerator Conference (EPAC'08)*, pp. 1056-1058, ISBN 978-92-9083-315-4, Genoa, Italy, June 23-27, 2008

Born, M. & Wolf, E. (1986). *Principles of optics.* (6th Edition), Pergamon, ISBN 0-08-026482-4, Oxford OX3 0BW, England

Bosch, R. A. (1999). Focusing of infrared edge and synchrotron radiation. *Nuclear Instruments and Methods in Physics Research A*, Vol.431, No.1-2, (July 1999), pp. 320-333, ISSN 0168-9002

Bowler, M.; Bahrdt, J. & Chubar, O. (2008). Wavefront propagation, In: *Modern developments in X-Ray and neutron optics,* Erko, A.; Idir, M.; Krist, T. & Michette, A. G., (Ed.), pp. 69-90, Springer, ISBN 978-3-540-74560-0, Berlin Heidelberg New York

Carr, G. L. & Dumas, P. (1999). *Accelerator-based Sources of Infrared and Spectroscopic Applications. Proceedings of SPIE,* Vol. 3775, (October 1999), ISBN 9780819432612

Chubar, O. V. (1995). Transverse electron beam size measurements using the Lloyd's mirror scheme of synchrotron light interference, *Proceedings of the sixteenth Particle Accelerator Conference (PAC'95)*, pp. 2447-2449, ISBN 0-7803-2937-6, Dallas, US, May 1–5, 1995

Chubar, O. & Elleaume, P. (1998). Accurate and efficient computation of synchrotron radiation in the near field region, *Proceedings of the sixth European Particle Accelerator Conference (EPAC'98)*, pp. 1177-1179, ISBN 0 7503 0579 7, Stockholm, Sweden, June 22-26, 1998

Chubar, O.; Elleaume, P. & Snigirev, A. (1999). Phase analysis and focusing of synchrotron radiation. *Nuclear Instruments and Methods in Physics Research A*, Vol.435, No.3, (October 1999), pp. 495-508, ISSN 0168-9002

Chubar, O.; Elleaume, P. & Snigirev, A. (2001). Phase corrections for synchrotron radiation. *Nuclear Instruments and Methods in Physics Research A*, Vol.467-468, No.1, (July 2001), pp. 932-935, ISSN 0168-9002

Clarke, J. A. (1994). A review of optical diagnostics techniques for beam profile measurements, *Proceedings of the fourth European Particle Accelerator Conference (EPAC'94)*, pp. 1643-1645, ISBN 9810219288, London, UK, June 27 – July 1, 1994

Coisson, R. & Marchesini, S. (1997). Gauss-Schell Sources as Models for Synchrotron Radiation. *Journal of Synchrotron Radiation,* Vol.4, No.5, (September 1997), pp. 263-266, ISSN 0909-0495

Duncan, W. D. & Williams, G. P. (1983). Infrared synchrotron radiation from electron storage rings. *Applied optics,* Vol.22, No.18, (September 1983), pp. 2914-2923, ISSN 1559-128X

Elleaume, P.; Fortgang, C.; Penel, C. & Tarazona, E. (1995). Measuring Beam Sizes and Ultra-Small Electron Emittances Using an X-ray Pinhole Camera. *Journal of Synchrotron Radiation,* Vol.2, No.5, (September 1995), pp. 209-214, ISSN 0909-0495

Fang, Z.; Wang, G.; Yan, X.; Wang, J.; Zhang, D.; Zhou, Y.; Zhao, F.; Xie, R.; Sun, B. & Wu, J. (1996). Monitoring the beam profile in HLS with synchrotron light. *Nuclear Instruments and Methods in Physics Research A*, Vol.370, No.2-3, (February 1996), pp. 641-643, ISSN 0168-9002

Ferrero, C.; Smilgies, D.-M.; Riekel, Ch.; Gatta, G. & Daly P. (2008). Extending the possibilities in phase space analysis of synchrotron radiation x-ray optics. *Applied Optics,* Vol.47, No.22, (August 2008), pp. E116-E124, ISSN: 1559-128X

Flanagan, J. W.; Hiramatsu, S. & Mitsuhashi, T. (1999). Optical Beamlines for the KEK B-Factory Synchrotron Radiation Monitors, *Proceedings of the eighteenth Particle Accelerator Conference (PAC'99)*, pp. 2120-2122, ISBN 0-7803-5573-3, New York, US, March 27 – April 2, 1999

Geloni, G.; Kocharyan V.; Saldin E.; Schneidmiller E. & Yurkov M. (2009a). Theory of edge radiation. Part I: Foundations and basic applications. *Nuclear Instruments and Methods in Physics Research A*, Vol.605, No.3, (July 2009), pp. 409-429, ISSN 0168-9002

Geloni, G.; Kocharyan V.; Saldin E.; Schneidmiller E. & Yurkov M. (2009b). Theory of edge radiation. Part II: Advanced applications. *Nuclear Instruments and Methods in Physics Research A*, Vol.607, No.2, (August 2009), pp. 470-487, ISSN 0168-9002

Grimm, O; Behrens, Ch.; Rossbach, J. & Schmidt, B. (2008). Longitudinal beam diagnostics application of synchrotron radiation at FLASH, *Proceedings of the eleventh European Particle Accelerator Conference (EPAC'08)*, pp. 1116-1118, ISBN 978-92-9083-315-4, Genoa, Italy, June 23-27, 2008

Guidi, M. C.; Piccinini, M.; Marcelli, A.; Nucara, A.; Calvani, P. & Burattini, E. (2005). Optical performances of SINBAD, the Synchrotron INfrared Beamline At DAFNE. *Journal of the Optical Society of America A,* Vol.22, No.12, (December 2005), pp.2810-2817, ISSN 1084-7529

Green, G.K. (1976). *Spectra and optics of synchrotron radiation.* Preprint BNL 50522, (April 15, 1976). Brookhaven National Laboratory, Associated Universities, Inc. Upton, New York, 11973

Hiramatsu, S.; Iwasaki, H.; Mitsuhashi, T.; Naitoh, T. & Yamamoto, Y. (1999). Measurement of small beam size by the use of SR interferometer, *Proceedings of the eighteenth Particle Accelerator Conference (PAC'99)*, pp. 492-494, ISBN 0-7803-5573-3, New York, US, March 27 – April 2, 1999

Hofmann, A. & Meot, F. (1982). Optical resolution of beam cross-section measurements by means of synchrotron radiation. *Nuclear Instruments and Methods in Physics Research*, Vol.203, No.1-3, (December 1982), pp. 483-493, ISSN: 0167-5087

Hs, I. C. & Huang, T. H. (1993). Design Study of Beam Profile Monitor of storage Ring by Using Synchrotron Radiation, *Proceedings of the fifteenth Particle Accelerator Conference (PAC'93)*, pp. 2465-2467, ISBN 0-7803-1203-1, Washington, D.C., US, May 17-20, 1993.

Ikemoto, Y.; Moriwaki, T.; Hirono, T.; Kimura, S.; Shinoda, K.; Matsunami, M.; Nagai, N.; Nanba, T.; Kobayashi, K. & Kimura, H. (2003). Infrared microspectroscopy station at BL43IR of Spring-8. Poster presentation at: *International Workshop on Infrared*

Microscopy and Spectroscopy with Accelerator Based Sources (WIRMS-2003), Lake Tahoe, California, US, July 8-11, 2003 Available from: http://infrared.als.lbl.gov/WIRMS/Presentations/SPring-8_poster1.pdf

Jackson, J. D. (1999). *Classical electrodynamics.* (3th Edition), John Wiley & Sons, Inc., ISBN 0-471-30932-X, New York, Chichester, Weinheim, Brisbane, Singapore, Toronto

Katoh, M. & Mitsuhashi, T. (1999). Measurement of beam size at the Photon Factory with the SR interferometer, *Proceedings of the eighteenth Particle Accelerator Conference (PAC'99)*, pp. 2307-2309, ISBN 0-7803-5573-3, New York, US, March 27–April 2, 1999

Kim, K.-J. (1986). Brightness, coherence and propagation characteristics of synchrotron radiation. *Nuclear Instruments and Methods in Physics Research A*, Vol.246, No.1-3, (May 1986), pp. 71-76, ISSN 0168-9002

Kimura, H.; Moriwaki, T.; Takahashi, S.; Aoyagi, H.; Matsushita, T.; Ishizawa, Y.; Masaki, M.; Oishi, S.; Ohkuma, H.; Namba, T.; Sakurai, M.; Kimura, S.; Okamura, H.; Nakagawa, H.; Takahashi, T.; Fukui, K.; Shinoda, K.; Kondoh, Y.; Sata, T.; Okuno, M.; Matsunami, M.; Koyanagi, R.; Yoshimatsu, Y. & Ishikawa, T. (2001). Infrared beamline BL43IR at SPring-8: design and commissioning. *Nuclear Instruments and Methods in Physics Research A*, Vol.467-468, No.1, (July 2001), pp. 441-444, ISSN 0168-9002

Kimura, S.; Kimura, H.; Takahashi, T.; Fukui, K.; Kondo, Y.; Yoshimatsu, Y.; Moriwaki, T.; Nanba, T. & Ishikawa, T. (2001). Front end and optics of infrared beamline at SPring-8. *Nuclear Instruments and Methods in Physics Research A*, Vol.467-468, No.1, (July 2001), pp. 437-440, ISSN 0168-9002

Kimura, S.; Nakamura, E.; Nishi, T.; Sakurai, Y.; Hayashi, K.; Yamazaki, J. & Katoh, M. (2006). Infrared and terahertz spectromicroscopy beam line BL6B(IR) at UVSOR-II. *Infrared Physics and Technology,* Vol.49, Nos.1-2 (September 2006), pp. 147-151, ISSN 1350-4495

Korchuganov, V.; Blokhov, M.; Kovalchuk, M.; Krylov, Yu.; Kvardakov, V.; Moseiko, L.; Moseiko, N.; Novikov, V.; Zheludeva, S.; Odintsov, D.; Rezvov, V.; Ushkov, V.; Valentinov, A.; Vernov, A.; Yudin, L. & Yupinov, Yu. (2005). The status-2004 of the Kurchatov center of SR. *Nuclear Instruments and Methods in Physics Research A*, Vol.543, No.1, (May 2005), pp.14-18, ISSN 0168-9002

Korchuganov, V. N. & Smolyakov, N. V. (2009). IR-UV edge radiation at Siberia-2 storage ring. *Nuclear Instruments and Methods in Physics Research A*, Vol.603, No.1-2, (May 2009), pp. 13-15, ISSN 0168-9002

Lopez-Delgado, R. & Szwarc, H. (1976). Focusing all the synchrotron radiation (2π radians) from an electron storage ring on a single point without time distortion. *Optics Communications,* Vol.19, No.2, (November 1976), pp. 286-291, ISSN 0030-4018

Miyahara, T. & Kagoshima, Y. (1995). Importance of wave-optical corrections to geometrical ray tracing for high brilliance beamlines. *Review of Scientific Instruments*, Vol.66, No.2, (February 1995), pp. 2164-2166, ISSN 0034-6748

Naito, T. & Mitsuhashi, T. (2010). Improvement of the resolution of SR interferometer at KEK-ATF dumping ring, *Proceedings of the first International Particle Accelerator*

Conference (IPAC'10), pp. 972-974, ISBN 978-92-9083-352-9, Kyoto, Japan, May, 23-28, 2010

Ogata, A. (1987). Focusing of synchrotron radiation. *Nuclear Instruments and Methods in Physics Research A*, Vol.259, No.3, (September 1987), pp. 566-575, ISSN 0168-9002

Ogata, A. (1991). On optical resolution of beam size measurements by means of synchrotron radiation. *Nuclear Instruments and Methods in Physics Research A*, Vol.301, No.3, (March 1991), pp. 596-598, ISSN 0168-9002

Paech, A.; Ackermann, W.; Weiland, T. & Grimm, O. (2006). Numerical simulation of synchrotron radiation for bunch diagnostics, *Proceedings of the tenth European Particle Accelerator Conference (EPAC'06)*, pp. 1031-1033, ISBN 92-9083-278-9, Edinburgh, Scotland, June 26-30, 2006

Paech, A.; Ackermann, W.; Weiland, T. & Grimm, O. (2007). Simulation of synchrotron radiation at the first bunch compressor of FLASH, *Proceedings of the twenty-second Particle Accelerator Conference (PAC'07)*, pp. 3925-3927, ISBN 1-4244-0917-9, Albuquerque, New Mexico, USA, June 25-29, 2007

Roy, P.; Rouzieres, M.; Qi, Z. & Chubar O. (2006). The AILES infrared beamline on the third generation synchrotron radiation facility SOLEIL. *Infrared Physics & Technology,* Vol.49, Nos.1-2, (September 2006), pp. 139-146, ISSN 1350-4495

Sabersky, A.P. (1973). The geometry and optics of synchrotron radiation. *Particle Accelerators,* Vol.5, (September, 1973), pp. 199-206, ISSN 0031-2460

Shintake, T. (2003). Real-time animation of synchrotron radiation. *Nuclear Instruments and Methods in Physics Research A*, Vol.507, No.1-2, (July 2003), pp. 89-92, ISSN 0168-9002

Smolyakov, N. V. (1998a) Interference diagnostics for storage ring electron beam. *Nuclear Instruments and Methods in Physics Research A*, Vol.405, No.2-3, (March 1998), pp. 229-231, ISSN 0168-9002

Smolyakov, N. V. (1998b) Wave-optical properties of synchrotron radiation. *Nuclear Instruments and Methods in Physics Research A*, Vol.405, No.2-3, (March 1998), pp. 235-238, ISSN 0168-9002

Smolyakov, N. V. (1998c) Wave-optical properties of synchrotron radiation and electron beam diagnostics, *Proceedings of the sixth European Particle Accelerator Conference (EPAC'98)*, pp. 1601-1603, ISBN 0 7503 0579 7, Stockholm, Sweden, June 22-26, 1998

Smolyakov, N. V. & Hiraya, A. (2005). Study of edge radiation at HiSOR storage ring. *Nuclear Instruments and Methods in Physics Research A*, Vol.543, No.1, (May 2005), pp. 51-54, ISSN 0168-9002

Takayama, Y.; Hatano, T.; Miyahara T. & Okamoto, W. (1998). Relationship between spatial coherence of synchrotron radiation and emittance. *Journal of Synchrotron Radiation*, Vol.5, No.4, (July 1998), pp. 1187–1194, ISSN 0909-0495

Takayama, Y.; Okugi, T.; Miyahara, T.; Kamada, S.; Urakawa, J.; Naito, T. (1999). Application limit of SR interferometer for emittance measurement, *Proceedings of the eighteenth Particle Accelerator Conference (PAC'99)*, pp. 2155-2157, ISBN 0-7803-5573-3, New York, US, March 27 – April 2, 1999

Tsien, R. Y. (1972). Pictures of dynamic electric fields. *American Journal of Physics,* Vol.40, No.1, (January 1972), pp.46-56, ISSN 0002-9505

Weitkamp, T.; Chubar, O.; Drakopoulos, M.; Souvorov, A.; Snigireva, I.; Snigirev, A.; Gunzler, F.; Schroer, C. & Lengeler, B. (2001). Refractive lenses as a beam diagnostics tool for high-energy synchrotron radiation. *Nuclear Instruments and Methods in Physics Research A*, Vol.467-468, No.1, (July 2001), pp. 248-251, ISSN 0168-9002

Williams, G. P. & Dumas, P. (1997). *Accelerator-Based Infrared Sources and Applications. Proceedings of SPIE,* Vol. 3153, (October 1997), ISBN 9780819425751

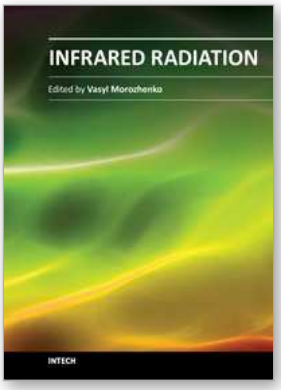

Infrared Radiation

Edited by Dr. Vasyl Morozhenko

ISBN 978-953-51-0060-7
Hard cover, 214 pages
Publisher InTech
Published online 10, February, 2012
Published in print edition February, 2012

This book represents a collection of scientific articles covering the field of infrared radiation. It offers extensive information about current scientific research and engineering developments in this area. Each chapter has been thoroughly revised and each represents significant contribution to the scientific community interested in this matter. Developers of infrared technique, technicians using infrared equipment and scientist that have interest in infrared radiation and its interaction with medium will comprise the main readership as they search for current studies on the use of infrared radiation. Moreover this book can be useful to students and postgraduates with appropriate specialty and also for multifunctional workers.

How to reference

In order to correctly reference this scholarly work, feel free to copy and paste the following:

Nikolay Smolyakov (2012). Wave Optics of Synchrotron Radiation, Infrared Radiation, Dr. Vasyl Morozhenko (Ed.), ISBN: 978-953-51-0060-7, InTech, Available from: http://www.intechopen.com/books/infrared-radiation/wave-optics-of-synchrotron-radiation

INTECH
open science | open minds

InTech Europe
University Campus STeP Ri
Slavka Krautzeka 83/A
51000 Rijeka, Croatia
Phone: +385 (51) 770 447
Fax: +385 (51) 686 166
www.intechopen.com

InTech China
Unit 405, Office Block, Hotel Equatorial Shanghai
No.65, Yan An Road (West), Shanghai, 200040, China
中国上海市延安西路65号上海国际贵都大饭店办公楼405单元
Phone: +86-21-62489820
Fax: +86-21-62489821